A statistical analysis of the mechanical and electronic-transport properties of stochastic porous fibrous materials

M. GRUJICIC*, C. L. ZHAO
Department of Mechanical Engineering, Program in Materials Science and Engineering, Clemson University, Clemson SC 29634
E-mail: mica.grujicic@ces.clemson.edu

W. N. ROY
Army Research Laboratory—Processing and Properties Branch, Aberdeen, Proving Ground, MD 21005-5069

Computer simulations are used to analyze mechanical and electronic-transport properties and their degradation in stochastic porous fibrous materials. Such materials are currently being used for electrochemical substrates in advanced battery technologies such as the nickel/metal-hydride and lithium-ion technologies. It is found that due a structural damage, material mechanical and electron-transport properties degrade during loading at a progressively higher rate leading ultimately to a complete loss of the material ability to support mechanical load or to conduct electrical current. A statistical sensitivity analysis is also developed which could be used in the design and fabrication of stochastic porous fibrous materials in order to ensure that a desired minimum level of the failure strength is attained at a sufficiently high probability. © *2005 Springer Science + Business Media, Inc.*

1. Introduction

Stochastic non-woven fibrous materials represent an important class of materials which are used as electrochemical substrates in advanced electrical battery technologies such as the nickels/metal-hydride (Ni/MH) and the lithium-ion (Li-ion) batteries. To achieve a high level of the mass-based energy density, the advanced battery technologies demand the use of low-density materials. Consequently, the electrochemical substrates are made of porous materials in which the volume fraction of the conductive material can be as low as 3%. The electrical conductivity of such highly-porous materials displays a typical *percolation* behavior. That is, when the constituent fibers form a continuous network, a high-conductivity path is created through the material imparting to it high electrical conductivity. Conversely, the absence of a such "*percolated*" network is associated with a negligible electrical conductivity of the porous fibrous materials.

Even when the porous fibrous materials are used for electrochemical substrates and thus are not required to carry mechanical loads during service, their mechanical properties are very critical since they may control the performance and the life cycle of the batteries. That is, electrochemical cycling (charging/discharging) gives rise to thermo-mechanical fatigue and, in turn, can lead to local material damage (primarily due to the failure of fiber/fiber bonds). This initially gives rise to

a gradual reduction in electrical conductivity, and can eventually lead to a complete loss of network connectivity and thus, to a loss of the required level of electrical conductivity. Thus, a better understanding of the micromechanics of fiber/fiber bond failure and of the associated degradation of electrical conductivity is very critical for the development of new electrochemical materials with enhanced electrical performance, superior degradation resistance and prolonged life cycle.

Micromechanics of the porous fibrous materials has been the subject of substantial research over the last three decades. In general, one can broadly divide the previous work on porous fibrous materials into four main categories: (a) continuum models based on the use of a unit cell [1]; (b) micro-mechanical models based on the use of average microstructural properties of the porous fibrous material [2]; (c) purely numerical models which utilize various network generation methods, and seek a continuum description of the porous fibrous material [3–5]; and (d) purely statistical models in which the progress of local failure is tracked in fibrous materials consisting of a regular arrangement of the fibers with statistically assigned material properties [6].

Recently, Sastry and co-workers [7–18] in series of paper introduced a new approach for analyzing the stochastic porous fibrous materials. The key feature of the approach developed by Sastry and co-workers [7–18] can be summarized as follows: (a) a statistics-based

Report Documentation Page

Public reporting burden for the collection of information is estimated to average 1 hour per response, including the time for reviewing instructions, searching existing data sources, gathering and maintaining the data needed, and completing and reviewing the collection of information. Send comments regarding this burden estimate or any other aspect of this collection of information, including suggestions for reducing this burden, to Washington Headquarters Services, Directorate for Information Operations and Reports, 1215 Jefferson Davis Highway, Suite 1204, Arlington VA 22202-4302. Respondents should be aware that notwithstanding any other provision of law, no person shall be subject to a penalty for failing to comply with a collection of information if it does not display a currently valid OMB control number.

1. REPORT DATE **2005**	2. REPORT TYPE	3. DATES COVERED **00-00-2005 to 00-00-2005**

4. TITLE AND SUBTITLE **A statistical analysis of the mechanical and electronic-transport properties of stochastic porous fibrous materials**		5a. CONTRACT NUMBER
		5b. GRANT NUMBER
		5c. PROGRAM ELEMENT NUMBER
6. AUTHOR(S)		5d. PROJECT NUMBER
		5e. TASK NUMBER
		5f. WORK UNIT NUMBER

7. PERFORMING ORGANIZATION NAME(S) AND ADDRESS(ES) **Celmson University,Department of Mechanical Engineering,Clemson,SC,29634**	8. PERFORMING ORGANIZATION REPORT NUMBER

9. SPONSORING/MONITORING AGENCY NAME(S) AND ADDRESS(ES)	10. SPONSOR/MONITOR'S ACRONYM(S)
	11. SPONSOR/MONITOR'S REPORT NUMBER(S)

12. DISTRIBUTION/AVAILABILITY STATEMENT
Approved for public release; distribution unlimited

13. SUPPLEMENTARY NOTES

14. ABSTRACT

15. SUBJECT TERMS

16. SECURITY CLASSIFICATION OF:			17. LIMITATION OF ABSTRACT	18. NUMBER OF PAGES	19a. NAME OF RESPONSIBLE PERSON
a. REPORT **unclassified**	b. ABSTRACT **unclassified**	c. THIS PAGE **unclassified**	**Same as Report (SAR)**	**10**	

network generation technique is used to capture the stochastic nature of the microstructure of the material; (b) rigidity of the fiber/fiber bonds is accounted for by assigning to the bonding (junction) points a torsional stiffness or thought the use of compliant zones adjacent to the junction points; (c) specific morphology-based material damage mechanisms consistent with the ones observed in the battery-substrate materials are implemented into the numerical model; and (d) aging of the substrate material is also considered by accounting for the changes in strength and/or stiffness of the fiber/fiber bonds resulting from dissolution and subsequent electro-redeposition of the conductive material.

In the present work, the computer simulation approach proposed by Sastry and co-works [7–18] has been combined with a statistical sensitivity analysis to address the issue of the design of stochastic porous fibrous materials which are optimized relative to obtaining a suitable combination of low density, high conductivity and low failure probability.

The organization of the paper is as follows: Details of the computer simulation procedure used to generate the microstructure and to determine mechanical and electrical responses of the stochastic porous fibrous materials are presented in Section 2. The main results obtained in the present work as well as the development of a statistical sensitivity analysis for the failure strength of stochastic porous fibrous materials are presented and discussed in Section 3. The key conclusions resulted from the present study are summarized in Section 4.

2. Computational procedure
2.1. Generation of the network
Two dimensional stochastic fiber networks used in the simulations of mechanical and electrical responses of the point-bonded fiber networks encountered in porous fibrous materials used as battery electrochemical substrates are generated using the procedure described below:

(a) First, the probability distribution functions (and their parameters) are selected for the key microstructure variables: fiber volume fraction, fiber orientation, fiber length, fiber center-point coordinates, and fiber length-to-diameter aspect ratio;

(b) Using the selected probability distribution functions, fibers are placed in a (square-shaped) unit cell, as shown schematically in Fig. 1a. The importance of the size of the unit cell used is discussed later;

(c) The intersection (bonding) points between the fibers are next determined and are treated as torsional junctions with a statistically assigned values of the torsional stiffness;

(d) Periodic boundary conditions are next applied by wrapping back into the unit cell the fiber segments which are located outside the cell boundaries, Fig. 1b. In other words, fiber segments exiting the cell across one boundary are allowed to reenter the same cell across the boundary which is parallel to the original boundary. This procedure prevents spurious edge effects from affecting the analysis and does not alter the selected
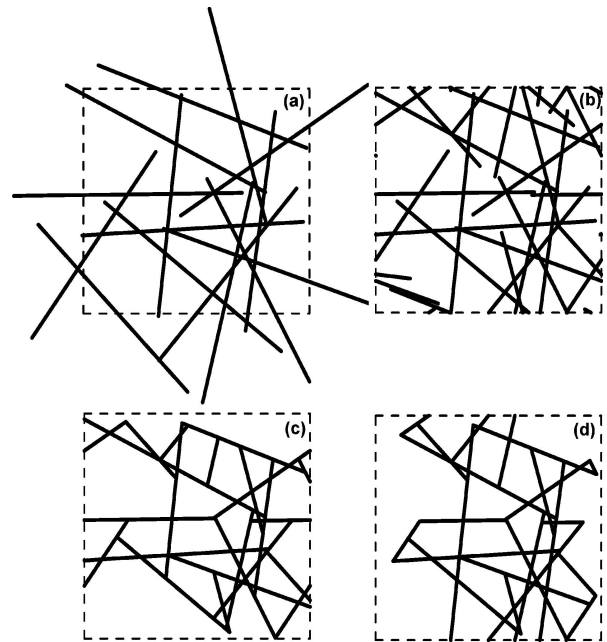

Figure 1 (a) Original network consisting of 15 randomly-oriented fibers of a uniform length equal to the unit cell edge length; (b) the corresponding network after the application of periodic boundary conditions; (c) and (d) the final (reduced) fiber networks obtained after (horizontal x-direction and vertical y-direction, respectively) non-load bearing fiber segments are removed.

value of a volume fraction of the fibers. Application of the boundary conditions, on the other hand, may reduce the average spacing between the junction points (i.e. the average segment length) and this phenomenon is examined more closely in the next section;

(e) Next, the fiber segments which do not carry a mechanical/electrical load in a particular (x or y) principal direction are removed. Such segments may belong to closed-loop network substructures which do not span the cell boundaries and also may include the "*dead-end*" segments. As shown in Fig. 1c–d, the final (reduced) fiber network depends on the loading direction.

Networks generated using the procedure described above have the following general features: (a) different realizations of the network associated with a fixed volume (or mass) fraction of the conducting phase contain generally different final (reduced) volume/mass fractions of the same phase; (b) while the network microstructures obtained are generally quite complex, they are largely non-triangulated and, hence, statically indeterminate; and (c) each network realization possesses unique conductivity and the statistical distribution of segment lengths. For example, the statistical parameters for the stochastic fibrous material displayed in Fig. 1c can be summarized as: fiber length-to-diameter aspect ratio, $l/d = 100$, (uniform) fiber length normalized by the unit cell length $= 1$, original fiber volume fraction (more precisely fiber area fraction within the present two dimensional analysis), $f_f = 11.78\%$, reduced volume fraction, $f_f^r = 7.57\%$, number of fiber/fiber bonding points $= 64$, average segment length normalized by the cell edge length $= 0.083$, and standard deviation of the normalized segment length $= 0.071$.
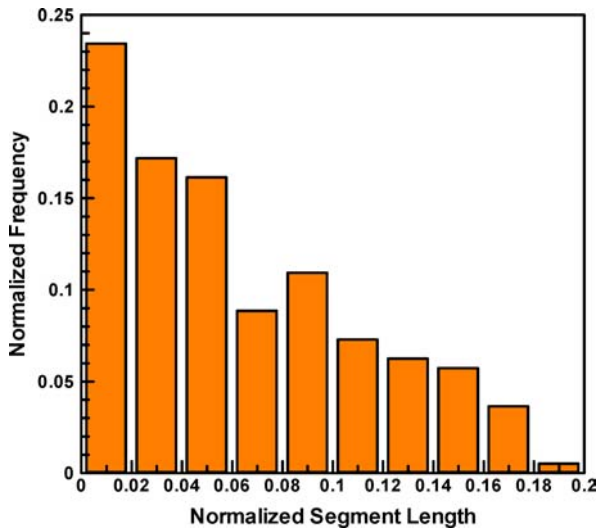
Figure 2 Frequency distribution plot for the fiber segment length normalized by the unit cell edge length for the network displayed in Fig. 1c.

It should be noted that the average segments length plays a critical role in the mechanical response of the stochastic fibrous materials analyzed in the present work. A segment-length frequency plot for the fiber network displayed in Fig. 1c is given in Fig. 2. This plot does not differ significantly for different realization of the network corresponding to a fixed value of the original volume fraction and a fixed value of the fiber aspect ratio. Conversely, significant variations occur when the original volume fraction and/or the aspect ratio are changed. Specifically, the frequency plots shifts forward the lower values of the segment lengths when the original fiber volume fraction and/or the fiber aspect ratio are increased. It should be noted that for a fixed unit cell edge length, an increase in the fiber aspect ratio, at a constant fiber diameter, is equivalent to an increase in the fiber (staple) length.

It should be also noted that the size of the simulation region (the unit cell) relative to the microstructural material scale could have a significant effect on the computed mechanical response of the stochastic fibrous materials. Specifically, if the unit cell is too small, the effective stiffness may be overestimated since the load would be born disproportionally by continuous individual fibers rather than by more compliant assemblies of fibers. However, this effect is somewhat mitigated by the use of periodic boundary conditions which tend to increase the number of fiber/fiber intersections and thus reduces the probability for individual fibers spanning the unit cell in the loading direction.

2.2. Beam assumptions

It is well established that the Euler-Bernoulli beam theory provides an excellent description of beams with a length-to-diameter aspect ratio greater than 5–10. However, some of the fiber segments in representative stochastic fibrous microstructures such as the ones displayed in Fig. 1a–b, have the aspect ratio significantly smaller than 5. Under such circumstances, the use of the Timoshenko beam theory is recommended to properly account for the deformation due to trans-

verse shear. This, in turn, helps prevent overestimation of the beam stiffness which generally results when the Euler-Bernoulli beam theory is used. However, the stiffness of an array of beams connected with flexible bonds (the approach used in the present work to model stochastic fibrous materials) has been found by Sastry and co-workers [7–18] not to be significantly affected by the choice of the beam theory. Sastry and co-workers [7–18] observed that the low-aspect-ratio segments (the ones in which the effect of transverse shear is most pronounced) are generally clustered and essentially function as rigid interconnect for the rest of the network composed of larger-aspect-ratio compliant fibers. It is, hence, readily understood why improvements in modeling the stresses at a beam length scale have a relatively weak effect on the mechanical response of stochastic fibrous material at the unit-cell length scale. Taking into consideration these findings of Sastry and co-worker [7–18], the computationally less-demanding Euler-Bernoulli beam theory is used in all the calculations carried out in the present work.

2.3. Failure criteria and network damage mechanism

In an assembly of connected segments such as the one used to represent stochastic fibrous materials, maximum stresses unavoidably occur at the segment junction (bonding) points. Following Sastry and co-workers [7–18], a maximum-stress failure criterion is utilized in the present work to model the progression of material damage during mechanical loading. As demonstrated in Fig. 3a–c, within such a damage mechanism, one can envision two extreme levels of damage tolerance by the porous fibrous material. A schematic of the undamaged fiber network is displayed in Fig. 3a in which segment 2 at the junction point B is assumed to be subject to a largest combined stress (defined as a square root of the sum of the squared normal stress and the maximum shear stress). When such a combined stress
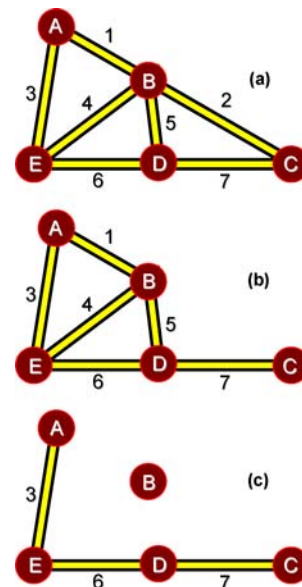

Figure 3 A schematic of two possible damage mechanisms in the porous fibrous materials; (a) undamaged network structure; (b) segment-failure based mechanism and (c) bonding-point-failure based mechanism.

in segment 2 at the junction point B exceeds the failure stress, one can either fail (i.e. remove) only segment 2, Fig. 3b, or (more conservatively) eliminate all the segments associated with node B. Simulations carried out by Sastry and co-workers [7–18] showed that the peak stress (can be treated as the failure strength of stochastic porous materials) is not very sensitive to the choice between these two damage mechanisms. While the junction-point failure mechanism, Fig. 3c, is generally computationally less demanding, the segment failure mechanism, Fig. 3b, is used in the present work since its implementation is much simpler.

2.4. Inter-fiber bonding

The mechanical response of the porous fibrous materials considered in the present work is greatly affected by the details of fiber/fiber bonding. These materials are generally processed by sintering and, hence, fiber/fiber junction points are normally not "*perfect*" in the sense that the joined fibers do not completely intersect one another. To quantify the extend of fiber/fiber intersections, Berhan and Sastry [7] introduced a so-called the "*degree-of-intersect*" parameter. For fibers with equal circular cross-sections, this parameter takes on a value between 0.5 (corresponds to the case when the fibers are just touching each other) to 1.0 (the case when the two fibers completely intersect each other). A detailed three-dimensional analysis of the mechanical response of the imperfect fiber/fiber junction points carried out by Berhan and Sastry [7] showed that torsional stiffness of such joints increases substantially with an increase in the magnitude of the degree-of-intersect parameter and with an increase in the magnitude of the angle of intersection between the fibers. In addition, it is found that the maximum stress levels in the fibers at the junction points obtained using a more accurate three dimensional finite element analysis are somewhat higher (by roughly a factor of 2) than their two-dimensional counterparts (such as the ones obtained in the present work).

In addition to the degree-of-intersect and intersect angle, other parameters may effect torsional stiffness of the fiber/fiber junction points. Among these is the number of fiber segments eminating from a given junction point. In the present two-dimensional analysis in which a maximum of two fibers are allowed to intersect at a given junction point, one can distinguish only three types of junctions, i.e. those with 2, 3, or 4 non-dead-end fiber segments eminating from it. A schematic of these three types of junction points is given in Fig. 4a–c, respectively. Dead-end segments (i.e. the segments with a free end) are denoted using a circle while non-dead-end segments using a triangle in Fig. 4a–c. In should be noted that torsional resistance of a fiber/fiber bonding point is not only depended on the rigidity of the bond, but also on the number of associated non-dead-end segments. To account for the fact that torsional rigidity of a fiber/fiber bonding point increases with the number of associated non-dead-end segments, the mean value of the torsional stiffness is assumed to be proportional to the number of associated non-dead-end segments reduced by one.
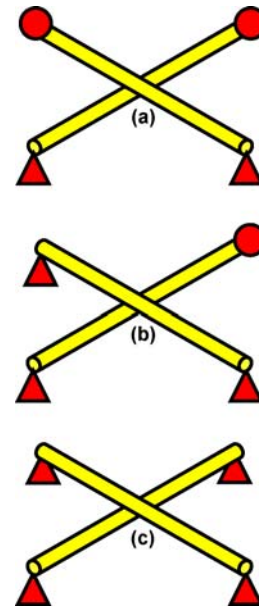

Figure 4 Three types of fiber/fiber bonds encountered in two-dimensional simulations of the porous fibrous materials. Circles are used to denote the dead-end segments while non-dead-end segments are denoted using triangles.

2.5. Finite element analysis of the mechanical response

Once a realization of the network microstructure is generated using the procedure described in Section 2.1, and torsional stiffness values are assigned to the fiber/fiber junction points following the procedure described in Section 2.4, a two-dimensional finite element analysis is carried out to determine the mechanical response of the material at hand in a given loading direction. The analysis is carried out under displacement-controlled boundary conditions within which the nodes on one of the edges of the unit cell normal to the loading direction are kept fixed while the nodes on the other edge (also normal to the loading direction) are assigned a constant displacement rate. The remaining nodes in the model are not subject to any constraints. Fiber segments are treated as one-dimensional Euler-Bernoulli-beam-type finite elements.

All the calculations are carried out by interfacing a general purpose mathematical/graphical package Matlab [20] with a general purpose finite element package Femlab [21]. In this approach, Matlab is used as pre-processing and post-processing modules while Femlab is used as a numerical solver module.

Standard mesh sensitivity and model robustness analyses were carried out following the procedure outlined in our recent work [22]. The results of these analyses validated that the model developed is mesh-insensitive and robust but the results will not be presented here for brevity.

2.6. Computation of electrical conductivity

Electrical conductivity of the stochastic porous fibrous materials is calculated using the SPICE 3 computer program which was originally created and currently maintained at the Electrical Engineering and Computer Science Department at the University of

California at Berkeley [19]. SPICE 3 is a general-purpose circuit simulation program for nonlinear *dc*, nonlinear transient, and linear *ac* analyses. Circuits analyzed may contain resistors, capacitors, inductors, mutual inductors, independent voltage and current sources, four types of dependent sources, lossless and lossy transmission lines, switches, uniform distributed *RC* lines, and the five most common semiconductor devices: *diodes*, *BJTs*, *JFETs*, *MESFETs*, and *MOSFETs*. The *dc* analysis portion of SPICE 3 used in the present work determines the *dc* operating point of a circuit in which inductors are shorted and capacitors opened. In order to eliminate unnecessary computation, all dead-end fiber segments as well as the segments intersecting the edges of the unit cell which are parallel with the direction of current flow are excluded during calculation of the electrical conductivity. A *dc* analysis is automatically performed prior to a transient analysis to determine the transient initial conditions, and prior to an *ac* small-signal analysis to determine the linearized, small-signal models for nonlinear devices. If requested, the *dc* small-signal value of a transfer function (ratio of output variable to input source), input resistance, and output resistance is also computed as a part of the *dc* solution. The *dc* analysis can also be used to generate *dc* transfer curves: a specified independent voltage or current source is stepped over a user-specified range and the *dc* output variables are stored for each sequential source value.

3. Results and discussion
3.1. Mechanical response and the progress of material damage

The unit cell and materials parameters used during the simulation of mechanical response which yielded the results displayed in Fig. 5a are given in Table I [7–18]. A typical uni-axial stress vs. uni-axial strain curve obtained during the simulations of mechanical response of the stochastic porous fibrous materials is displayed
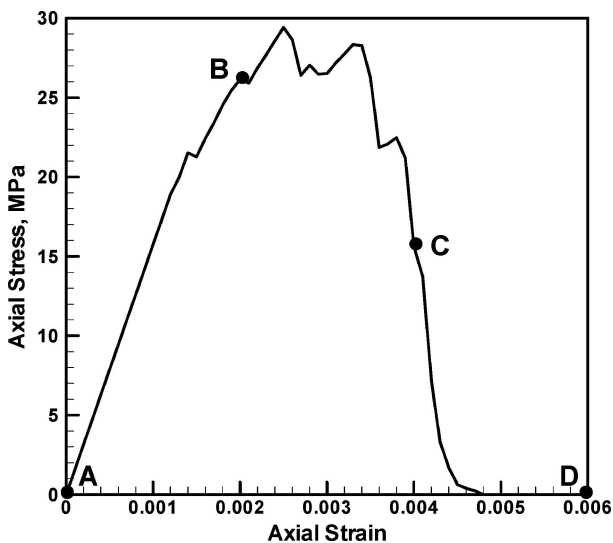
Figure 5 Evolution of a normalized electrical conductivity as a function of the uni-axial strain in the nickel-fiber based porous material displayed in Fig. 6a whose microstructural parameters are summarized in Table I.

T A B L E I Microstructural and materials parameters for the nickel-based porous fibrous material whose mechanical and electronic-transport responses are displayed in Fig. 5 and the microstructure in Fig. 6

Parameter	Symbol	Units	Mean value	Standard deviation
Unit cell edge width	l_{cell}	m	3.0×10^{-3}	0
Unit cell edge length	l_{cell}	m	3.0×10^{-3}	0
Nickel fiber diameter	d	m	3.0×10^{-5}	0
Nickel fiber length	l_f	m	3.0×10^{-3}	4.5×10^{-5}
Nickel fiber volume fraction	f_f	N/A	0.15	0
Nickel Young's modulus	E	Pa	2.10×10^{11}	0
Nickel Poission's ratio	ν	N/A	0.3	0
Nickel failure strength	σ_f	Pa	5.4×10^{8}	0
Nickel electrical resistance	ρ	Ωm	1.0×10^{-7}	0

in Fig. 5a. The stress is defined as a ratio of the applied load pre unit cell depth and the unit cell edge length.

The results displayed in Fig. 5a show that initially the uni-axial stress vs. uni-axial strain relation is nearly linear. Small non-linearity observed is a result of the failure of few highly stressed fiber segments. It should be noted that only elastic deformations are considered during modeling of the materials response since, due to a relatively low stress levels at which failure of the fiber segments occurs, the role of plasticity is deemed insignificant.

As loading proceeds in Fig. 5a, non-linearity between the stress and the strain increases and, occasionally, the stress drops. These stress drops are associated with a simultaneous failure of several fiber segments. At the largest levels of the stress, stress increase due to the incremental loading is roughly compensated by the structural material weakening due to the failure of an increasing number of fiber segments. Once the rate of structural weakening exceeds the rate of incremental loading, the stress level begins to drop dramatically and, ultimately, the porous fibrous material completely looses the ability to support load (the axial stress becomes zero).

The results displayed in Fig. 5a show that for the fiber network realization at hand, the peak uni-axial stress is $\sigma_{peak} \approx 29$ MPa and it occurs at a uni-axial-strain of about 0.25%, while the material looses its load-carrying capacity at a strain of approximately 0.5%.

The evolution of the fibrous material network during loading in the (horizontal) *x*-direction is displayed in Fig. 6a–d. The four networks shown in Fig. 6a–d correspond, respectively, to the uni-axial stress/uni-axial strain levels denoted as A–D in Fig. 5. It should be noted that in order to improve clarity of the networks displayed in Fig. 6a–d, failed fiber segments are not displayed. In addition, a magnification factor of 10 is applied to the horizontal component of the displacement in Fig. 6b–d.

An evolution of the electrical conductance of the porous fibrous material (Fig. 6a) during uni-axial loading in the (horizontal) *x*-direction is displayed in Fig. 7. The electrical conductance is normalized by that of a single nickel fiber with a length equal to the unit cell edge length and the diameter of 30 μm. The electrical conductance of such a fiber is 0.7854 Ω^{-1}. A
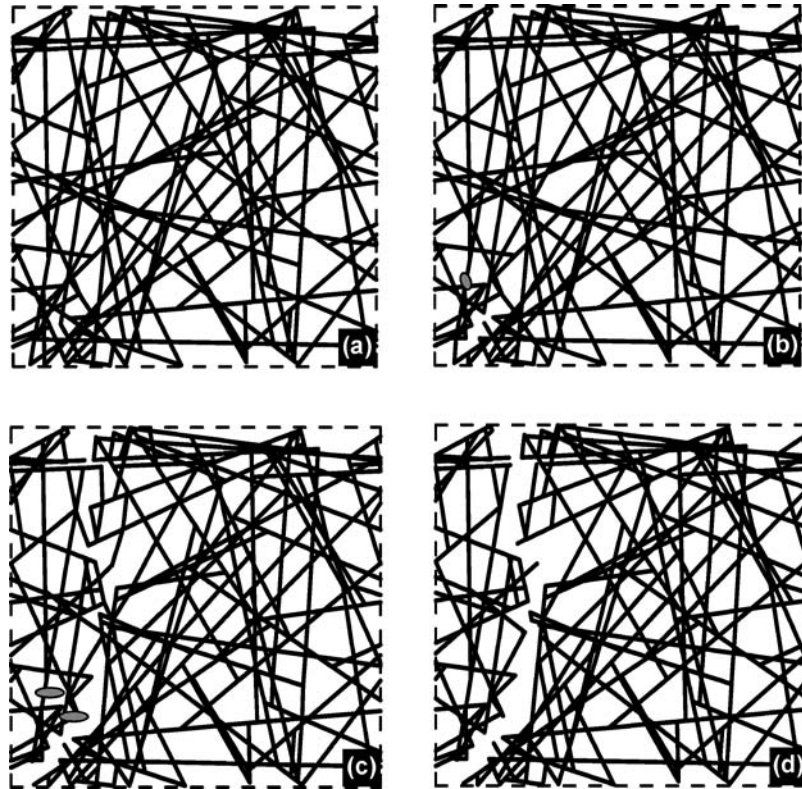
Figure 6 Evolution of the fiber network during uni-axial loading in the horizontal *x*-direction. Failed fiber segments are not shown to enhance clarity of the material damage. Networks (a)–(d) correspond to the uni-axial stress/uni-axial strain levels denoted as A–D in Fig. 5a.
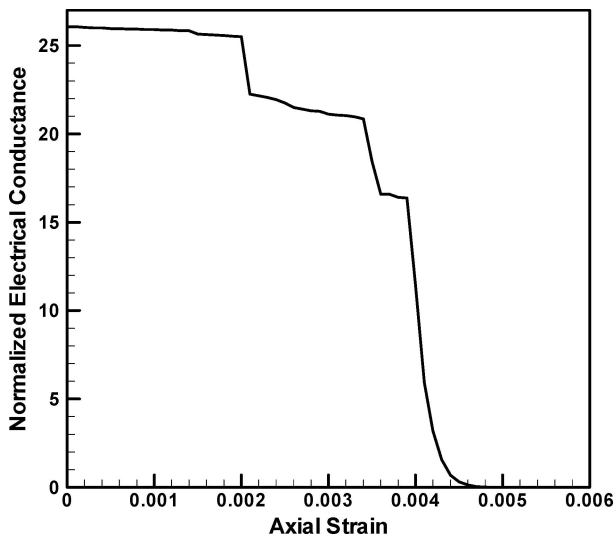

Figure 7 Evolution of a normalized electrical conductivity as a function of the uni-axial strain in the nickel-fiber based porous material displayed in Fig. 6a whose microstructural parameters are summarized in Table I.

comparison of the results displayed in Figs 5 and 7 and Fig. 6a–d shows that there is a direct correlation between the progress of the material damage, the materials ability to support load (as measured by the uni-axial stress) and the materials ability to transport electrical charge (as measured by its electrical conductance).

3.2. Effect of the unit cell edge length
The mean fiber diameter and the mean fiber length-to-diameter aspect ratio define the natural material microstructural length scale. When carrying out the com-

puter simulations of mechanical or physical responses of the materials with an irregular stochastic microstructure, one of the key issues is to identify an optimum size of the representative material element (a unit cell in the present case). If such a material representative element is chosen as too small, it will not realistically represent the actual material response. This may be particularly pronounced in the present case since the use of periodic boundary condition could give rise to an un-physical increase in the number of fiber/fiber bonding points. Also, in the limit of a very small size of the representative material elements, material response would be un-realistically dominated by individual fiber segments spanning the material representative element rather than by the assemblies of fiber segments. In the other extreme, the selection of a unit cell which is too large may increase the computation time so much that one may be prevented from assessing the complete statistics of the materials response (for stochastic materials such as the ones studied in the present work, the knowledge of the average materials properties may not be sufficient since such properties may be associated with relatively broad distributions).

To identify an optimum size of the unit cell, computer simulations of the mechanical response are carried out for a stochastic fibrous material with a fixed fiber diameter, fiber length and fiber volume fraction but for various values of the unit-cell edge length. An example of the results obtained is displayed in Fig. 8 in which the peak uni-axial stress is plotted as a function of the unit cell edge length. The error bars shown in Fig. 8 correspond to the $\pm$ one standard deviation range of the peak stress. The results displayed in Fig. 7 show that at
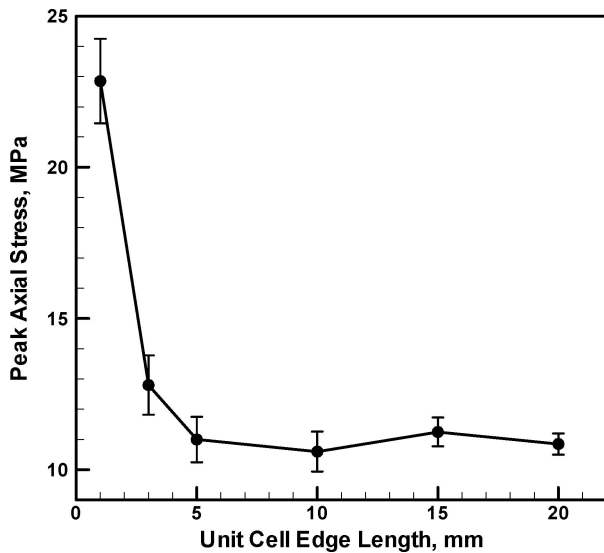
Figure 8 A typical effect of the unit-cell edge length on the peak uni-axial stress.

unit cell edge lengths in excess of approximately 5 mm, the mean value of the peak stress is not very sensitive to the choice of the unit cell edge length. In addition and as expected, as the unit cell edge length increases the standard deviation of the peak stress decrease since a continuously large volume of the material is being sampled. Following the findings resulted from the results displayed in Fig. 8, all the subsequent simulations are carried out using a unit-cell edge length of 5 mm.

3.3. Statistical analysis of the peak stress

Based on the results displayed in Fig. 5, it is clear that a porous fibrous material continues to degrade at a progressively higher rate once the applied stress reaches the peak stress of the material. Therefore, the peak stress can be considered as the effective failure strength of such materials and should be used as a key input parameter in the design of novel materials for electrochemical substrates in advanced batteries.

The main parameters which affect the magnitude of failure strength of the stochastic porous fibrous materials at hand are: fiber area fraction, f_f, fiber length-to-diameter aspect ratio, l_f/d, and torsional stiffness of fiber/fiber junction points, K_s. In addition, the magnitude of failure strength is affected by the stochastic nature of the network-like material microstructure. Due to the stochastic nature of the materials at hand, an analysis of its failure strength must ultimately answer a question like: "For a given type of fibers (characterized by the distributions of their diameter, aspect ratio and material properties), and a given porous fibrous material manufacturing process (which controls porous-material microstructure and the distribution of fiber/fiber junction-point torsional stiffness), what is the (nominal) volume fraction of the fiber phase needed to ensure that the failure strength of the resulting porous fibrous material is greater or equal to a target value with a high probability (say 99%). In addition, the analysis should provide a quantitative assessment of the sensitivity of the failure strength to variations in the ma-

terials and microstructural parameters (f_f, l_f/d, and K_s). To answer such questions, a statistical approach must be taken when analyzing the failure strength of the stochastic porous fibrous materials. An overview of a statistical sensitivity analysis and its application to the failure strength in these materials is presented in this section.

In general, the statistical sensitivity analysis deals with the problem of assessing sensitivity of the output of a mathematical model (used to represent a physical system) to variations in the model inputs (parameters, variables and assumptions). As stated above, the model output in the present work is the peak stress while the most important model inputs are: fiber volume fraction, fiber aspect ratio, fiber/fiber bond torsional stiffness and fibrous-material microstructure network. For simplicity, the model output will be denoted as y while the model inputs constitute a k-dimensional vector $\mathbf{x} = (x_1, \ldots, x_k)^T$ where superscript T is used for denote a vector/matrix transpose.

Function $y = f(\mathbf{x})$ (the peak stress) can be evaluated using a numerical approach (the finite element method in the present work), but generally, this function is not known in a closed form. However, the computed values of this function, $y_i = f(\mathbf{x})$ ($i = 1, n$, where n is the number of numerical evaluations) can be used in conjunction with a statistical approach such as the least-squares method to determine an approximate fitting function $\hat{f}(\mathbf{x})$ such that $y = \hat{f}(\mathbf{x}) + e = f(\mathbf{x})$ where the error, e, is often found to be associated with a normal distribution and to be independent of the model input, $\mathbf{x}$.

Components of the model input, $\mathbf{x}$, vary in accordance with their respective (known) probability distribution functions (typically an independent uniform or a correlated normal distribution function). When independent uniform distributions are used, the input parameters can be chosen so that they are uncorrelated at a level of the parent probability distribution function, $p(\mathbf{x})$. However, to ensure that the same uncorrelation, i.e. orthogonality is obtained at a level of the particular Monte Carlo sample, the sampled vectors of uniform variable ξ_i ($i = 1, n$) should be transformed into the corresponding orthogonal sample vector $\mathbf{x}$ as:

$$\mathbf{x}_i = \hat{\Sigma}^{1/2} \xi_i \qquad (1)$$

where $\hat{\Sigma}$ is the sample correlation matrix.

When the model input is sampled from a correlated multivariate normal distribution function with a covariance matrix Σ and an expectation value η, a vector ξ of independent standard normal variables with zero mean and unit variance is first generated and then converted into the corresponding correlated vector $\mathbf{x}$ as [22]:

$$\mathbf{x} = \eta + \Sigma^{1/2} \xi. \qquad (2)$$

In the present work, the three input parameters (fiber volume fraction, fiber aspect ratio and fiber/fiber bond torsional stiffness) are each assigned several (mean) values in the respective ranges of interest and an uncorrelated normal distribution (with a fixed variance). The

Parameter	Symbol	Units	Mean values	Standard deviation
Fiber volume fraction	f_f	N/A	0.05, 0.1, 0.15	0.01
Fiber aspect ratio	l_f/d	N/A	50, 75, 100	10
Junction-point torsional stiffness	K_s	N·m	0.0001	0.00002

values of the model input distribution parameters used are given in Table II.

Once the input parameters are orthogonalized using the procedure described above, the numerical model is solved for each of n Monte Carlo input samples (n should be a large number to ensure a statistically large sample) to yield $y_1 = f(\mathbf{x}_1), \ldots, y_n = f(\mathbf{x}_n)$. A value of $n = 100$ is used in the present work for each combination of the mean values of the three input parameters.

Next, before the linear regression analysis is applied to the computed y_i values, a post-simulation input transformation, $u = u(\mathbf{x})$ is generally used to convert the input parameters into the appropriate orthogonal polynomials. In the present model, these polynomials are selected to include the input parameters themselves, their squares and two parameter products. A linear regression analyses is then applied to the model output as:

$$y = \sum_j \beta_j u_j + e \tag{3}$$

where j is the transformed input-parameter index and β's the linear regression coefficients determined using the standard least-squares methodology.

Next, when the components of the vector u are uncorrelated (as is the present case), uncertainty of the model output (as measured by the variance σ_y^2) can be defined as:

$$\sigma_y^2 = \sum_j \beta_j^2 \sigma_{u_j}^2 + \sigma_e^2 \tag{4}$$

The same expression, Equation 4, can be used to compute the sample variances, S_y^2, $S_{u_j}^2$ and S_e^2 (while using the same denominator $1/(n-1)$ during calculation of these variances) again provided the input parameters are uncorrelated.

Finally, a statistical sensitivity index, SI_j, for the input parameter u_j can be defined as:

$$SI_j = \beta_j^2 \frac{S_{u_j}^2}{S_y^2} \tag{5}$$

and can be used to quantify the sensitivity of the model output to variations in this input parameter.

Application of the linear regression analysis to the numerically computed failure strength data of 500 runs,

$\hat{\sigma}_f$, yielded the following relationship:

$$\hat{\sigma}_f = 36.04 f_f - 96.78 \cdot 10^{-4} \frac{l_f}{d} + 6.817 \cdot 10^4 K_s$$

$$+ 52.3 f_f^2 + -14.86 \cdot 10^{-7} \left(\frac{l_f}{d}\right)^2$$

$$- 93.57 \cdot 10^6 K_s^2 - 0.1565 f_f \frac{l_f}{d} + 3098 f_f K_s$$

$$+ 2.442 \frac{l_f}{d} K_s \tag{6}$$

A correlation between the numerically-computed σ_f data their corresponding analytical counterparts $\hat{\sigma}_f$ is given in Fig. 9a. It is seen that there is a very good correlation between the two sets of failure strength data with the correlation coefficient $R^2 = 99.17\%$. A frequency plot for the failure-strength residuals (errors) defined as a $\hat{\sigma}_f - \sigma_f$ difference is displayed in Fig. 9b. A probability density function plot for a normal distribution with the identical variance as the frequency plot is also shown in Fig. 8b. It is seen that the residual (error) distribution is nearly normal. This is confirmed
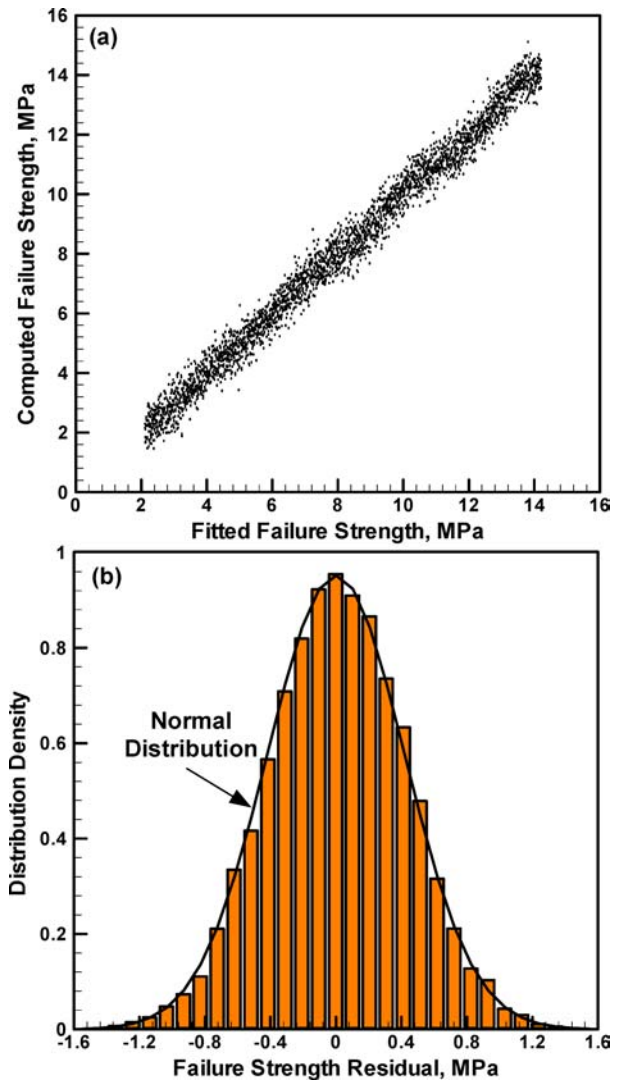

Figure 9 (a) A correlation between the fitted and numerically computed values of the failure strength and (b) Probability-distribution (frequency) plot for the failure strength residuals.

quantitatively by computing the skewness, s_k, and the kurtosis, k_k, for the frequency plot shown in Fig. 9b. The values obtained, $s_k = 0.05$ and $k_k = 3.09$, are found to be very near their normal distribution counterparts, $s_k = 0.0$ and $k_k = 3.0$. This finding may be related to the fact that the input data were sampled from a normal distribution.

Values of the statistical sensitivity index SI_j for the nine for transformed input parameters computed using Equations 4 and 5 show that the fiber/fiber junction-point torsional-stiffness ($SI_3 = 0.4810$) and the fiber volume fraction ($SI_1 = 0.4117$) have the largest effect on the statistical variability of the failure strength. The sum of the statistical sensitivity indices for the remaining six transformed input parameters is 0.0848.

Now that an analytical function for the effects fiber volume fraction, fiber length-to-diameter aspect ratio and fiber/fiber junction-point torsional stiffness on the failure strength and the associated error distribution function are determined, one may proceed with answering the original question regarding the fiber volume fraction needed to obtain a desired minimum level of the failure strength with a specific probability in a fibrous porous material with given mean values and given variances for the fiber aspect ratio and the torsional stiffness. For example, for a material consisting of the nickel fibers with mean aspect ratio of 75 and a mean value of the torsional stiffness of 1.0. $\times 10^{-4}$ N · m, if the desired failure strength is say $\hat{\sigma}_f = 10$ MPa the use of these data and Equation 6 yields a mean value of the required fiber volume fraction $f_f = 0.149$. However, it should be noted that since the failure strength at a given mean value of the three input parameters is found to be associated with a normal distribution, the computed fiber volume fraction $f_f = 0.149$ ensures that the required minimum failure strength $\hat{\sigma}_f = 10$ MPa is obtained with a probability of only 50%. Since electrochemical substrates are generally designed for a small probability of failure, one needs to determine the fiber volume fraction which will yield the same failure strength $\hat{\sigma}_f = XX$ MPa but at a high (say 99%) probability. The probability of 99% corresponds to a failure stress level which is 2.58 standard deviations away from the mean failure strength. This means that in order to obtain a failure strength of 10 MPa with a probability of 99%, one needs to determine the volume fraction which will yield a mean value of the failure strength of $10 + 2.58 \times 0.423 = 11.09$ MPa, where 0.423 MPa corresponds to (computed) failure-strength standard deviation. The use of Equation 6 now yields the fiber volume fraction $f_f = 0.175$.

To summarize, under the conditions of fixed standard deviations of the input parameters (fiber volume fraction, fiber length-to-diameter aspect ratio and fiber/fiber junction-point torsional stiffness), it is found that the failure strength can be represented using a linear combination of the orthogonal linear and nonlinear polynomials based on these input parameters. In addition, the error between the accurate numerical and approximately analytical values of the failure strength is found to be associated with a normal distribution. Under such circumstance, one can approach the design of stochastic porous fibrous materials on a statistical bases and provide a procedure for ensuring that the resulting material will have a desired level of the probability of survival (as measured to be the probability that the material will possess a failure strength whose magnitude is greater or equal to a desired level).

For the three input parameters considered in the present work, it is assumed that their mean values and standard deviations can be controlled within the ranges indicated in Table II. Since the materials at hand are generally processed using paper manufacturing technologies, control of the mean volume fraction within a range of ±1% is deemed achievable. Likewise, a control of the fiber aspect-ratio distribution within ±10 (which translates into a control of the fiber length with ±3·10⁻⁴ m) is generally attainable through conventional fiber sifting and screening processes. A control of the torsional stiffness of fiber/fiber junction points is most challenging and it is carried out through a strict control of the sintering process parameters. At present, no correlation has been established between the sintering process parameters and the resulting distribution of the junction-point torsional stiffness. It must be noted that establishment of such relationships in a prerequisite for the full utilization of the material design methodology presented in the present work. This is particularly the case considering the observed large value of the statistical sensitivity index of the torsional stiffness.

4. Conclusions
Based on the results obtained in the present work, the following main conclusions can be drawn:

1. A two-dimensional finite element analysis can be used to study the deformation behavior including the progress of structural material damage due to the failure of bonded fiber segments in stochastic porous fibrous materials such as Ni-based mats used as electrochemical substrates in advanced nickel/metal-hydride batteries.

2. The progress of the structural material damage leads initially to a gradual and subsequently to a precipitous reduction in electrical conductivity in these materials culminating in a total loss of electrical conductivity when the damage causes a complete loss in connectivity at the fibrous network.

3. Due to the stochastic character of materials microstructure and variability in materials properties, a statistical approach is required when analyzing the failure strength in these materials. In other words, similarly to ceramic materials, stochastic porous fibrous materials are designed to possess, at a specified high probability, a desired minimum level of the failure strength.

References

1. R. E. MERIDITH and C. W. TOBIAS, "II Conduction in Heterogeneous Systems," Advances in Electrochemistry and Electrochemical Engineering, Interscience, New York. (1962) p. 15.
2. J. W. S. HEARLE, in "The Mechanics of Dense Fibre Assemblies," The Mechanics of Flexible Fibre Assemblies, edited by J. W. S. Hearle, J. J. Thwaites and J. Amichayal (Sijthoff and Noordholf, New York, 1980) p. 51.
3. W. LU, L. A. CARLSSON and Y. ANDERSON, *Tappi J.* **78** (1995) 155.
4. W. LU and L. A. CARLSSON, *ibid.* **79** (1996) 203.
5. W. LU, L. A. CARLSSON and A. DE. RUVO, *ibid.* **79** (1996) 197.
6. W. A. CURTIN, *J. Mater. Res.* **5** (1990) 1549.
7. L. BERHAN and A. M. SASTRY, *J. Comp. Mater.* **37** (2003) 715.
8. C. W. WANG, K. A. COOK and A. M. SASTRY, *J. Electrochem. Soc.* **150** (2003) A385.
9. Y. B. YI and A. M. SASTRY, *Phys. Rev. E* **66** (2002) 1.
10. A. M. SASTRY, C. W. WANG and L. BERHAN, *Key Engng. Mater. Trans. Tech. Publ.* **200** (2001) 229.
11. X. CHENG, A. M. SASTRY and B. E. LAYTON, *ASME J. Engng. Mater. Techn.* **123** (2001) 12.
12. C. W. WANG, L. BERHAN and A. M. SASTRY, *ibid.* **122** (2000) 450.
13. C. W. WANG and A. M. SASTRY, *ibid.* **122** (2000) 460.
14. C. W. WANG, X. CHENG, A. M. SASTRY and S. B. CHOI, *ibid.* **121** (1999) 503.
15. X. CHENG, C. W. WANG, A. M. SASTRY and S. B. CHOI, *ibid.* **121** (1999) 514.
16. X. CHENG and A. M. SASTRY, *Mech. Mater.* **31** (1999) 765.
17. A. M. SASTRY, S. B. CHOI and X. CHENG, *ASME J. Engng. Mater. Techn.* **120** (1998) 280.
18. A. M. SASTRY, X. CHENG and C. W. WANG, *J. Therm. Comp. Mater.* **11** (1998) 288.
19. Spice 3, http://www.eecs.berkeley.edu/.
20. MATLAB, 6th Edition, "The Language of Technical Computing," The MathWorks Inc., 24 Prime Park Way, Natick, MA, 01760-1500, 2000.
21. www.comsol.com, FEMLAB 2.3a, COMSOL Inc., Burlington, MA 01803, 2003.
22. M. GRUJICIC and K. M. CHITTAJALLU, *Appl. Surf. Sci.* **227** (2004) 56.